Journal of Power Sources 195 (2010) 6549–6558

Contents lists available at ScienceDirect

Journal of Power Sources

journal homepage: www.elsevier.com/locate/jpowsour

An integrated modeling approach for temperature driven water transport in a polymer electrolyte fuel cell stack after shutdown

Manish Khandelwal[1], M.M. Mench*

Fuel Cell Dynamics and Diagnostics Laboratory, Department of Mechanical and Nuclear Engineering, The Pennsylvania State University, University Park, PA 16802, USA

ARTICLE INFO

Article history:
Received 11 March 2010
Received in revised form 26 April 2010
Accepted 26 April 2010
Available online 26 May 2010

Keywords:
Polymer electrolyte fuel cell
Shutdown
Thermo-osmosis
Heat-pipe
Water transport
Stack

ABSTRACT

The concept of using controlled temperature gradients to non-parasitically remove excess water from porous media during PEFC stack shutdown has been numerically investigated. An integrated modeling approach focusing both at stack and single cell level is presented. The stack thermal model is developed to obtain detailed temperature distribution across the PEFC stack. The two-phase unit fuel cell model is developed to investigate the detailed water and thermal transport in the PEFC components after shutdown, which for the first time includes thermo-osmotic flow in the membrane. The model accounts for capillary and phase-change induced flow in the porous media, and thermo-osmotic and diffusive flow in the polymer membrane. The single cell model is used to estimate the local water distribution with land or channel boundary condition, and the experimentally validated stack thermal model provided the transient temperature boundary conditions. Two different stack designs are compared to quantify the residual water in the stack. Model results indicate that a favorable temperature gradient can be formed in the stack to enhance the water drainage rate, esp. at anode end cell locations, where freeze/thaw damage has been observed to occur.

1. Introduction

Improvement in the fuel cell durability and rapid cold start performance are two key technical challenges that impede successful fuel cell commercialization for automobile application. Both topics have gained considerable attention in last 5 years [1–4] and strongly depend on the water management scheme in the fuel cell and stack. After cell/stack shutdown, water will redistribute in the fuel cell components depending on the cell materials, stack design, and shutdown protocol. All these factors determine the residual water and its movement in the fuel cell components.

Recent studies performed by Mench and co-workers have shown that residual water plays a key role in freeze-damage [4–7] and fuel cell cold start ability [8–10]. Khandelwal et al. [8–9] have shown that if not purged, almost 15–20% of the total energy required to achieve successful cold start can be consumed in melting ice. Studies performed by Kim and Mench [4] have identified various physical degradation modes and have shown that liquid water in contact with the catalyst layer must be minimized to mitigate damage. Currently, various purging methods are being utilized to minimize the residual water in the fuel cell. In practice, purge is traditionally restricted to a short duration due to the high parasitic energy requirement.

Recently, non-parasitic purging methods using temperature gradients [11–12] have gained attention as a potential pathway to non-parasitically reduce the residual water saturation. Bradean et al. [11] and Perry et al. [12] have shown that a modest temperature gradient can induce significant liquid water motion after shutdown. Perry et al. [12] observed that in some cases, the anode end cells can have substantially lower performance compared to cathode end cells, due to the different direction of liquid water transport during cool down to a frozen state. It was found that this water movement direction was dependent on the temperature gradient in the end cell. This observation is consistent to our model results reported in a previous publication [13]. In this case, the cathode side of anode end cell remains at a higher temperature than the anode side during cool down, resulting in higher liquid water at cathode catalyst layer. To solve this, Perry et al. [12] used different diffusion media with lower permeability at anode end cells. This helped to restrict motion of liquid into the catalyst layer from the porous plates and prevent damage. An advantage of this approach is that it can be selectively used for any cells in the stack. On the other hand, Bradean et al. [11] changed the stack design such that a favorable temperature gradient is setup in the stack, i.e. the anode bi-polar plate temperature is higher than

* Corresponding author. Tel.: +1 814 865 0060; fax: +1 814 863 4848.
E-mail address: mmm124@psu.edu (M.M. Mench).
[1] Current address: UTC Power Corporation, South Windsor, CT 06074, USA.

0378-7753/$ – see front matter © 2010 Elsevier B.V. All rights reserved.
doi:10.1016/j.jpowsour.2010.04.080

Nomenclature

A	cross-sectional area (m^2)
b	height of the stack (m)
C_p	specific heat ($J\,kg^{-1}\,K^{-1}$)
D	diffusion coefficient ($m^2\,s^{-1}$), thermo-osmotic diffusion coefficient ($mol\,m^{-1}\,s^{-1}\,K^{-1}$)
EW	equivalent weight ($kg\,mol^{-1}$)
H_{gl}	latent heat of vaporization ($J\,kg^{-1}$)
k	permeability (m^2), thermal conductivity ($W\,m^{-1}\,K^{-1}$)
M	molecular weight ($kg\,mol^{-1}$)
P_{sat}	saturation pressure (Pa)
R	universal gas constant ($8.314\,J\,mol^{-1}\,K^{-1}$)
s	saturation
t	time (s)
T	temperature (K)
u	velocity ($m\,s^{-1}$)

Subscript

amb	ambient air
bp	bi-polar plate
m	membrane
w	liquid water phase, water in Nafion

Latin symbol

ρ	density ($kg\,m^{-3}$)
ε	porosity
μ	viscosity (Pa s)
λ	water content in Nafion ($mol\,H_2O/mol\,SO_3^-$)

the cathode bi-polar plate temperature for all cells in the stack. This will result in similar water drainage from porous media into the flow channels in all cells. The disadvantage of this approach is that it requires changes in the stack design and can't be selectively used for anode end cells in the stack. In spite of this experimental evidence, temperature gradient driven flow is not very well understood in the fuel cell literature. Recently, the authors developed a two-phase single cell model for PEFC shutdown and investigated the thermal driven mode of water transport in fuel cell [13–14]. The novel feature of their model was inclusion of a directly measured thermo-osmosis relationship in the electrolyte membrane and the phase-change induced (PCI) transport [15–16] in the porous media. Previous work was limited to a constant temperature gradient condition and is currently extended to a simulated shutdown scenario in this work.

In this work, the two-phase single cell model is extended to explore the concept of using controlled temperature gradients to non-parasitically remove excess water from end cells during PEFC stack shutdown. To explore this concept, an integrated modeling approach focusing on both single cell and stack is adopted. The single cell model is used to estimate the local water distribution with land/channel boundary condition, and the stack thermal model provides the transient temperature boundary condition to simulate the end cells. Ultimately, the proposed methodology can be used to improve stack design and develop shutdown protocol to minimize the residual water.

2. Model development

This section provides brief description of both the two-phase single cell and stack thermal models. Detailed formulation of both models has been published elsewhere [8,13–14].

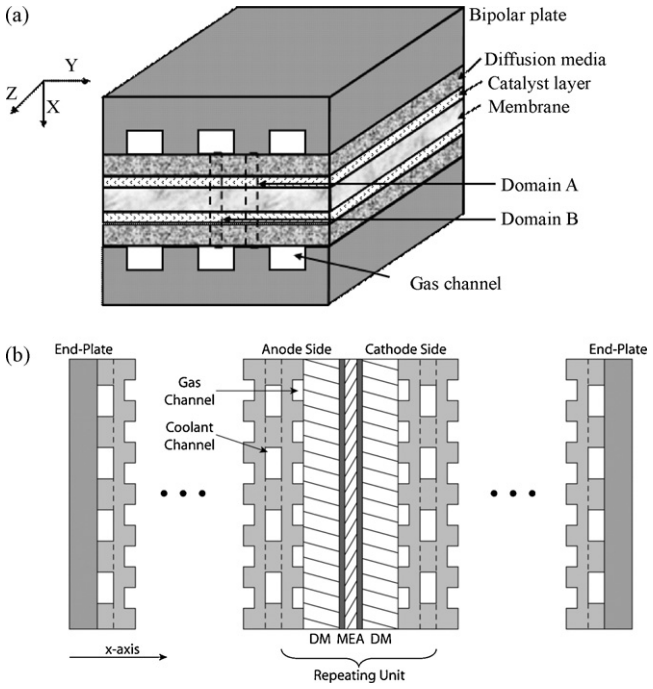

Fig. 1. (a) Schematic and control volume for the two-phase single cell computational model. Computational domain with both land (Domain A) and channel (Domain B) boundary condition are shown. (b) Schematic of the PEFC stack and its components for one-dimensional stack thermal model [8].

2.1. Two-phase single cell model

A schematic of the fuel cell, its components, and control volume for the two-phase single cell model development is shown in Fig. 1a. Conservation of mass and energy has been performed for each fuel cell component and combined with various interfacial boundary conditions [13–14]. In this model, diffusion media (DM) and catalyst layers (CLs) are considered to be porous media and the polymer electrolyte membrane (Nafion®) is considered to be water solvent. Another key assumption is that the polymer electrolyte membrane is treated with a diffusion model. The diffusion model is chosen based on the availability of experimental water diffusivity data. The water content of membrane, λ, is defined as the number of moles of water associated with a mole of sulfonic acid group in the membrane H_2O/SO_3^-. By using the gradient of λ as the driving force, the diffusion model can be used for the whole range of $0 < \lambda < \lambda_0 = 22$. Actually, if the polymer membrane can be considered as a porous media with free water at a high water content (i.e. $22 > \lambda > 14$), through the capillary relation for a two-phase flow in porous media, we can show $\nabla p_w \sim (\partial p_w/\partial s_w)\nabla s_w \sim \nabla\lambda$. Thus the hydraulic-type model can be simplified to a diffusion-type model, providing unification of the two approaches [5]. The model accounts for capillary and phase-change induced (PCI) flow (heat-pipe effect) [13,16] in the porous media, thermo-osmotic and diffusive flow in the polymer membrane. Other model assumptions and detailed derivation for water and thermal transport have already been presented by Khandelwal et al. [13]. For brevity, only a summary of model is presented in this article.

In the porous media (DM and CL), the governing equation for water transport can be written as

$$\varepsilon\rho_w \frac{\partial s_w}{\partial t} - \rho_w \nabla\left(\left(k_{rw}\frac{k}{\mu_w}\right)\nabla p_w\right) - \nabla(D_{gT}\nabla T) = 0 \quad (1)$$

where

$$D_{gT} = D\frac{M_w}{R}\frac{\partial}{\partial T}\left(\frac{P_{sat}}{T}\right) \quad (2)$$

where s_w is the liquid water saturation, p_w is liquid water pressure, D is water vapor diffusion, P_{sat} is saturation pressure and T is temperature of the control volume. All other symbols are defined in the Nomenclature. In Eq. (1), the first term represents the rate of change of water in the control volume, the second and third terms represent the capillary transport and diffusion flux due to the phase-change effect, respectively. It should be noted that in this formulation, the phase-change induced (PCI) flow is driven purely by thermodynamic saturation pressure gradients. It does not include surface energy effects that may also play an important role, but have yet to be investigated in fuel cell components. Eq. (1), along with the saturation and capillary relation is solved for liquid water saturation and pressure in the porous media domain.

For the Nafion® domain, water transport is modeled with a pure diffusion model [17–19], including thermo-osmosis [20–21]. Water transport in the membrane can be represented in terms of membrane water content (λ_w) and the governing equation can be written as [13]:

$$\frac{\partial \lambda_w}{\partial t} = \nabla(D_\lambda \nabla \lambda_w) + \left(\frac{EW}{\rho_m}\right) \nabla(D_T \nabla T) \tag{3}$$

where D_λ is the membrane water diffusion coefficient, EW is membrane equivalent weight, ρ_m is membrane density, and D_T is the membrane thermo-osmotic diffusion coefficient. In Eq. (3), the first term on right hand side represents the diffusion flux and second term is due to the thermo-osmotic flux. It should be noted that by using the gradient of water content, λ (water concentration) as the driving force, the diffusion model can be used for the whole range of $0 < \lambda < \lambda = 22$ to treat the liquid water [13].

The energy equation may also have different forms in various fuel cell components. For the porous media, the generalized energy equation can be written as [13]:

$$\frac{\partial(\overline{\rho C_P} T)}{\partial t} + \rho_w C_{p,w} \nabla(u_w T) = \nabla(k \nabla T) + S_{vap} H_{gl} \tag{4}$$

where ρ, C_p and k are porous media density, specific heat and thermal conductivity. In Eq. (4), the left most term represents the rate of change of energy in the control volume (i.e. thermal energy storage), and second term represents the advection due to liquid water, the first term on the right is the conduction heat transfer and last term represents the heat released/absorbed due to the phase-change in the porous media. Advection transport due to the vapor diffusion is neglected. Thermal transport properties for the DM were obtained by volume averaging. For the electrolyte domain (Nafion® or Gore® Membrane), conduction is the dominant mode of thermal transport. In the absence of any heat generation from phase-change, the energy equation can be written as [13]:

$$\frac{\partial(\rho C_p T)}{\partial t} + \rho_w C_{p,w} \nabla(u_w T) = \nabla(k \nabla T) \tag{5}$$

where all symbols are defined in the Nomenclature. The membrane thermal properties can also be evaluated as a mixture of dry membrane and water by volume averaging [7].

Water and thermal transport equations were solved in the DM, CL and membrane. Boundary/interface conditions need to be specified in the thru-plane direction (x-direction) only. Boundaries in other direction are symmetric; hence all gradients on these boundaries are zero. For water transport, zero mass flux is specified for a land boundary condition. For a channel boundary simulation, zero capillary pressure was specified in the gas channel. This channel boundary condition simulates the maximum drainage from the gas channel [13]. At the other porous material interfaces (DM|CL, DM|MPL, MPL|CL), mass flux and water pressure continuity is imposed. For the thermal transport, a constant temperature or convective boundary condition can be specified at the DM boundary (both at land/channel case). For all other interfaces in the computational domain, temperature and flux continuity is imposed.

2.2. Stack thermal model

The schematic of the stack and its components for the model development is shown in Fig. 1(b). The stack model used in this study was originally developed by Khandelwal et al. [8] for the cold start analysis and has been customized to simulate the shutdown scenario. The original stack cold start model [8] was a transient conduction heat transfer model with phase-change of ice, coolant re-circulation, advection heat transport due to flow of reactant gases, and heat generation due to the electrochemical reaction and ohmic losses. In this stack model, each stack component was resolved spatially in the x-direction, and conservation of energy is performed to obtain the final governing equation for the temperature. To modify this stack start-up model for a shutdown scenario, reactant gas and coolant flow was eliminated and no heat generation due to electrochemical reaction or melting of ice was considered. Additionally, advection heat transfer due to the liquid motion under temperature gradient is also neglected. Thus, the only mode of heat transfer across the solid stack components in the PEFC shutdown model is conduction. The generalized governing equation for each stack component can be written as

$$\frac{\partial T}{\partial t} = \left(\frac{k}{\rho C_p}\right) \frac{\partial^2 T}{\partial x^2} \tag{6}$$

where all symbols are defined in the Nomenclature. In Eq. (6), the left side is the rate of change of control volume temperature (i.e. thermal energy storage), right side is the conduction heat transfer. Interface temperature and flux continuity was imposed across all stack components, and convective boundary condition was used at both end plates. Details of numerical implementation are provided in Refs. [8,28].

2.3. Model integration

To estimate the residual water in the anode/cathode end cell, an integrated approach combining the stack thermal model and two-phase single cell model is adopted. A flow chart describing the adopted integrated approach is shown in Fig. 2. The transient stack thermal model provides the spatial temperature distribution, which is used to obtain the temperature boundary condition for single cell model. This temperature boundary condition can be obtained for any cell in the stack. In this study only anode and cath-

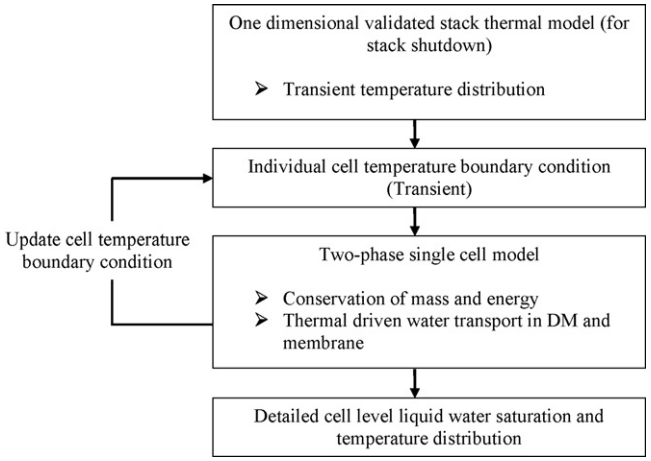

Fig. 2. Flowchart illustrating the integrated modeling approach combining stack thermal model with two-phase single cell model.

Table 1
Stack and cell parameters used in model simulation.

Symbol	Parameter (unit)	Value [Ref]
l	Width of the stack (m)	0.1
b	Height of the stack (m)	0.25
N	Number of cells	20
t_{ep}	End plate thickness (m)	0.005 (Design 1) 0.05 (Design 2)
t_{cp}	Coolant plate thickness (m)	0.0008
t_{bp}	Bi-polar plate thickness (m)	0.0008
t_{dm}	Anode/cathode DM thickness (μm)	400
t_{cl}	Anode/cathode CL thickness (μm)	10
t_m	Membrane thickness (μm)	20
$k_{p,DM}$	DM permeability (m^2)	3×10^{-12} [22,23]
$k_{p,CL}$	CL permeability (m^2)	3×10^{-14} [5]
ε_{DM}	DM porosity	0.8
ε_{CL}	CL porosity	0.3
s_{irr}	Irreducible saturation	0.35, assumed
D_λ	Membrane water diffusion coefficient ($m^2\ s^{-1}$)	2×10^{-10} [24]
D_T	Membrane thermo-osmotic diffusion coefficient (mol/ms K)	$-1.04 \times 10^{-3}\ e^{(-2297.3/T)}$ [25]
EW	Membrane equivalent weight ($kg\ mol^{-1}$)	1.1
H_{gl}	Latent heat of vaporization ($J\ kg^{-1}$)	2260×10^3 [26]
T_{amb}	Ambient temperature (K)	298

ode end cells are investigated. Using the cell temperature boundary condition, the single cell model is used to estimate the local water distribution with land/channel boundary condition.

During shutdown, the stack temperature will decrease from normal operating condition to room temperature. Therefore, the temperature boundary condition from the stack model will be transient in nature. It should be noted that the model integration was done in an explicitly rather than a real time fashion due to numerical complexity. To numerically implement this model integration, transient temperature conditions from the stack model were stored. As the solution marches in time, the temperature boundary condition in the single cell model was updated from the stored temperature information from the stack simulations. The time to reach the steady state condition (temperature only) will depend on the stack design and material properties.

3. Result and discussion

Stack dimensional parameters and material properties are listed in Tables 1 and 2, respectively.

3.1. Model validation

3.1.1. Two-phase single cell model

The single cell model was qualitatively validated for phase-change induced flux (PCI) [13] in the DM. For qualitative validation, the model was run on a test configuration of 4 layers sandwiched DM and observations were compared with neutron-radiography (NR) studies. The model was simulated with land and channel boundary condition, with different temperature gradient and average temperatures. These detailed PCI flux studies have already been presented elsewhere [13,28]. Only one result of transient liquid temperature distribution in the 4 layers sandwiched DM is shown in Fig. 3. Fig. 3 shows a transient profile of liquid saturation distribution in the 4 layered sandwiched diffusion media with land boundary condition, for two different temperature differences (ΔT = 10 and 2 °C). These two temperature differences provide two extreme cases (ΔT = 0.5 and 2.5 °C across each DM) to investigate the PCI effect in the DM. Initial liquid saturation of 0.2 was specified and average temperature was maintained at 75 °C in both scenarios. With a land boundary condition, liquid water will evaporate on the left side and will diffuse towards the right (due to lower temperature/concentration), and can condense anywhere inside the DM or on the right wall. As the configuration marches forward in time, liquid saturation on left side decreases to zero and a dry front moves toward the right. On the other hand, condensed water on right side will increase the liquid saturation and eventually increase to a value greater than the irreducible saturation. As liquid saturation value exceeds the irreducible saturation value, a dominating backward capillary flow is developed, and eventually, a steady state condition can be achieved when evaporation and vapor diffusion towards right will be balanced by the backward capillary flux. Comparing Fig. 3a and b, it can also be observed that with change of temperature gradient across DM, only the time scale of diffusion process (phase-change flux) changes. For ΔT = 10 °C, steady state condition is achieved in almost 300 s, as shown in Fig. 3a. However, for ΔT = 2 °C, a steady state condition was not achieved until 900 s (Fig. 3b). At steady state, the liquid saturation profile will be same for both cases, but the time to reach steady state can be dramatically different.

To qualitatively validate the model trend and results, neutron-radiography (NR) imaging was used. The NR imaging experiments were performed at the National Institute of Standards and Technology (NIST) test facility, where a small field-of-view (2.5 cm^2) high resolution (~10 μm) neutron imaging system exists. Details of the text fixture and experimental methodology are presented elsewhere [28]. To observe the PCI effect as simulated, 4 layers of commercial diffusion media (SGL® series 10BB/10BA/10BA/10BB)

Table 2
Thermal/material properties of the stack components.

	Thermal conductivity, k (W/m K)	Density, ρ ($kg\ m^{-3}$)	Specific heat, C_p (J/kg K)
End plate	10 [26]	1740 [26]	1460 [26]
Coolant plate	10 [26]	1400 [26]	935 [26]
Bi-polar plate	10 [26]	1400 [26]	935 [26]
Diffusion media	0.4 [27]	450	710 [26]
Catalyst layer	0.2 [27]	450	710 [26]
Membrane	0.2 [27]	1980 [24]	1170 [26]

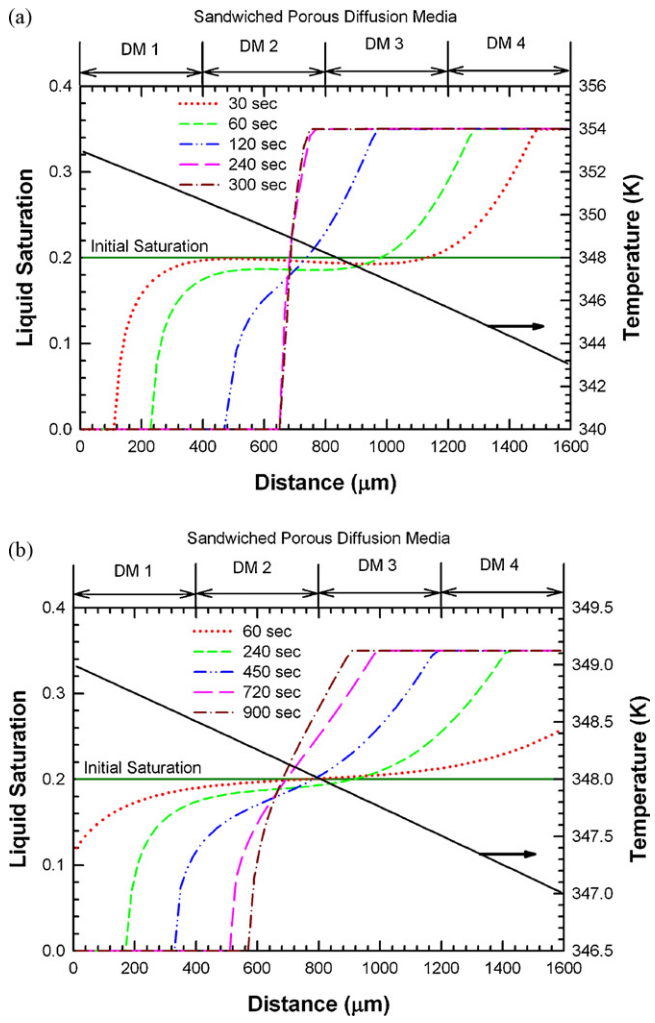

Fig. 3. Transient liquid saturation distribution in 4-layer sandwiched diffusion media at different times T_{avg} = 75 °C, land boundary condition (a) ΔT = 10 °C and (b) ΔT = 2 °C.

were used for the experimentation. In a non-operating condition, anode side gas channels were filled with liquid water and a temperature gradient was applied by two coolant re-circulation baths [28,29]. The anode bi-polar plate (left side in Fig. 4) was maintained at 70 °C and the cathode bi-polar plate (right side) was maintained at 60 °C. Microporous layers were turned to be facing both channel sides to prevent liquid water penetration into the DM (breakthrough pressure is measured to be ~6 kPa), but allow vapor diffusion. Fig. 4 shows the NR images at 1, 5 and 16 min after the start of the experiment. After 1 min of experimentation (Fig. 4a), it can be clearly seen that water has condensed on the cathode side from the anode channel. The condensed water has moved underneath the cathode land or began to drain inside the channel (top/bottom wall of cathode gas channel). Without an imposed temperature gradient, no water transport across the cell was observed. This observation is quite similar to that predicted from the one-dimensional model. At t = 5 min, more water has condensed underneath the land and drained inside the cathode gas channel (Fig. 4b). From Fig. 4c, it can be seen that the cathode gas channel is almost filled with liquid water after 16 min of the experiment. It should be noted that in the NR imaging experiments, the anode gas channel was always filled with liquid water, i.e. it has an infinite source of water to evaporate. On the other hand, in the numerical simulation, the amount of water is limited by the specified initial condition. Thus, no dry front movement can be observed from the NR imaging.

3.1.2. Stack thermal model

As previously mentioned in Section 2.2, the stack model was originally developed for cold start analysis and is modified here for the shutdown scenario. During model development for cold start analysis, the stack thermal model was validated with the start-up experimental data on a 20-cell stack from −10 °C to ambient temperature. The stack was fully instrumented to measure operating current density, individual cell voltage for all 20 cells, and temperatures measurements for 1st, 5th, 10th, 15th and 20th cell. After a rigorous sensitivity study, the model was validated for all 5 locations temperature measurement [28]. Further details of stack validation cannot be provided due to stack propriety information. Moreover, stack model calibration is true for one set of stack dimension and need to be recalibrated, if the stack dimensions and materials are changed. In the result section, we have used the stack dimension and material properties that are available in the published literature.

3.2. Impact of thermo-osmosis

To investigate the effect of thermo-osmosis on water transport, one-dimensional simulations were performed on a full cell geometry. Before simulating the real shutdown temperature conditions from stack model, simulations were performed with constant temperature gradient and average temperature. Applying these constant temperature conditions help in understanding how temperature affects water transport in the cell. These conditions also represent the maximum impact of thermo-osmosis on water removal after cell shutdown. Thermo-osmosis has not traditionally been included in fuel cell models, but can become an important mode of water transport under shutdown conditions, as described below.

Simulation dimensions and other parameters are shown in Table 1. The average temperature was maintained at 75 °C and two different ΔT: 10 and 2 °C across the fuel cell were used. Simulations are presented with constant temperature and land boundary condition with $T_L = T_{avg} + \Delta T/2$, $T_R = T_{avg} - \Delta T/2$, where T_L is the anode side temperature and T_R is the cathode side temperature. It has already been shown that the trend for water transport with land and channel boundary condition is similar [13]. Moreover, with land a boundary condition it is relatively easy to monitor the water transport, as no vapor or liquid can escape the computational domain. Initial temperature, liquid saturation in DM and CL, and membrane water content is specified as a value of T_L, 0.15, and 15.2 ($14 + 8s_w$), unless otherwise specified. The thermo-osmotic diffusion coefficient is negative for most commonly used fuel cell membranes. A typical range of thermo-osmotic diffusion coefficient is 10^{-6} to 10^{-7} mol m^{-1} s^{-1} K^{-1} [25], depending on the membrane average temperature. The expression shown in Table 1 has been determined for a W.L. Gore® membrane [25].

Fig. 5(a) and (b) shows the transient liquid saturation/water content profile in a fuel cell with a negative thermo-osmotic diffusion coefficient for ΔT = 10 and 2 °C, respectively. With negative thermo-osmotic diffusion coefficient, the direction of thermo-osmotic flux in the membrane will be from the cold to hot side, i.e. from cathode catalyst layer to anode catalyst layer, as simulated here. However, diffusion flux will be from the anode to cathode side. So, the direction of net water flux in membrane will depend on the relative magnitude of diffusion flux (positive direction) and thermo-osmotic flux (negative direction). For a given membrane, the magnitude of these fluxes will depend solely on a coupled balance between the concentration and temperature gradient effects, respectively. As the temperature field is developed in the domain,

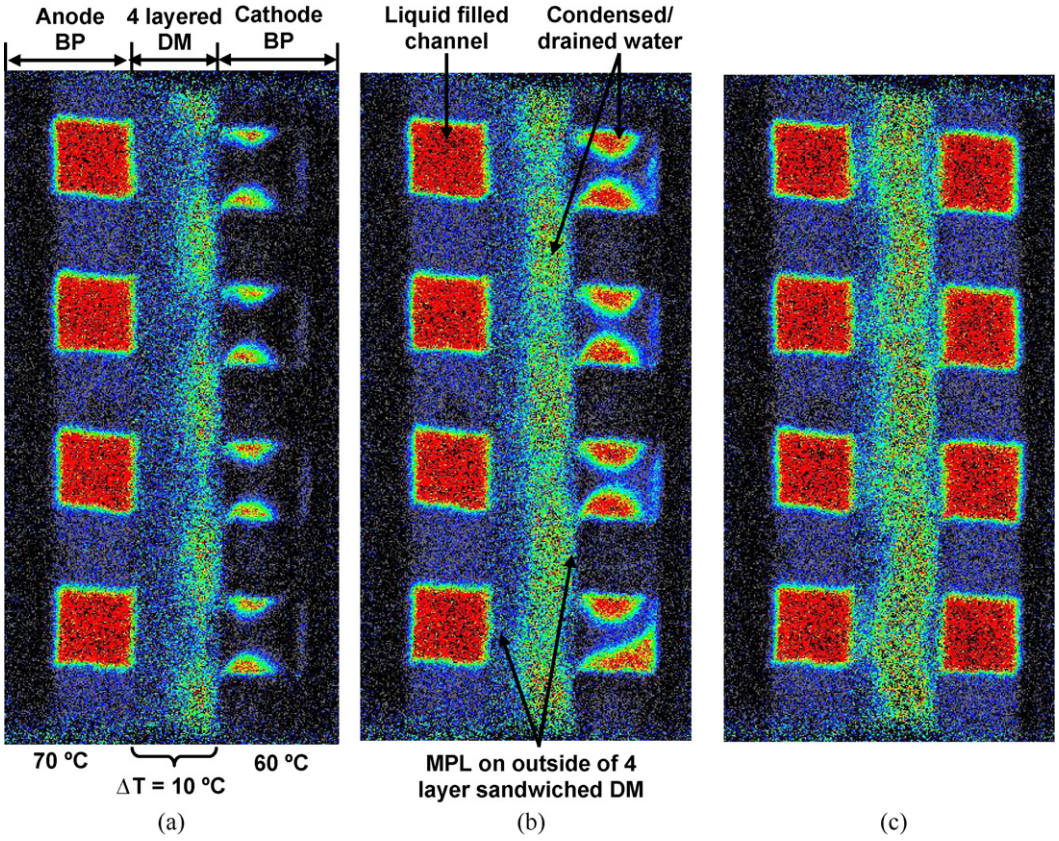

Fig. 4. Neutron-radiography images showing the PCI effect across a 4-layer sandwiched diffusion media: SGL® series 10BB/10BA/10BA/10BB, T_{avg} = 65 °C, ΔT = 10 °C (a) t = 1 min, (b) t = 5 min and (c) t = 16 min.

thermo-osmotic flux will remove water at a constant rate from the cathode to anode side of the membrane. However, due to phase-change induced flux in the DM and CL, liquid saturation on the anode catalyst layer increases. On the cathode catalyst layer, the liquid saturation is decreasing with time. The magnitude of the diffusion flux will be increasing as the concentration gradient increases across the membrane. Fig. 5(a) shows a scenario (ΔT = 10 °C), when the diffusion flux cannot overcome the opposing thermo-osmotic flux due to high temperature gradient. In this case, as soon as cathode catalyst layer is dried, no water can be transported from anode to cathode or vice-versa. Thus, in this scenario the membrane becomes a barrier for water drainage and both anode and cathode DM and CL will behave as two disjoint porous media domains. It should be noted that the thermo-osmotic fluxes deducted by Kim and Mench [25] were for fully liquid saturated membranes, and it is likely that for partially dry membranes, thermo-osmotic flux is reduced somewhat. Fig. 5(b) shows another scenario (ΔT = 2 °C) when diffusion flux is able to overcome the opposing thermo-osmotic flux. It has been already shown that in the porous media (DM and CL), decreasing the average temperature will slow rate of water vapor diffusion [13]. Thus, implying that diffusion flux in membrane can reach the same order as the previous scenario ΔT = 10 °C. However, thermo-osmotic flux in the membrane will be drastically reduced due to the decrease in the temperature gradient across membrane. As we can see from the plot, initially, liquid saturation near the anode catalyst layer increases and then it start decreasing as water diffuses from anode to the cathode side. At the same time, the liquid saturation at the cathode catalyst layer reduces to zero, as liquid water was transported to anode catalyst layer by thermo-osmotic flux along with the water movement towards the land by phase-change induced flux. Also, the net rate of water transport across the membrane (from anode CL to cathode CL) is lower than the amount of water which can be removed from PCI effect at cathode CL. Thus, the cathode catalyst layer will remain dry. Another important aspect is that all the water from the anode cannot be transported to cathode side. At steady state, a balance of diffusion flux and thermo-osmotic flux in the membrane will be achieved and no more water can be transported. So, in this scenario, the cathode CL can achieve the dry condition and anode CL will always have some residual water. The amount of residual water can be estimated by the flux balance. For example in the ΔT = 2 °C scenario, thermo-osmotic flux is $\sim 2.65 \times 10^{-4}$ kg m^{-2} s ($\Delta T_{\text{membrane}} \sim 0.2$ °C). From the diffusion flux relation $D_\lambda M_W(\rho_m/EW)(\Delta\lambda_W/\Delta x)$ and with $s_w = 0$ ($\lambda_w = 14$) on the cathode catalyst layer side, it can be found that residual liquid saturation on the anode side should be around 0.102. A typical temperature difference across any cell in a conventional stack PEFC stack can vary from 0 to 2 °C depending on the cell location in the stack. However, with the change in the stack design (e.g. Bradean et al. [11]) and shutdown protocol (e.g. forced cooling on one end during shutdown [28]), the temperature gradient across the cells can be substantially increased. Study of water transport in end cell and impact of stack design on water drainage etc. is presented in the following sub-section.

3.3. Stack temperature distribution

In this study, two different 20-cell stack designs proposed by Bradean et al. [11] are investigated for end cell water transport and are shown in Fig. 6. In the first design (Design 1), the stack is insulated from all sides except the cathode end plate (Fig. 6a), thus artificially creating a defined temperature gradient. In Design 2, a heat reservoir is attached between the end plate and insulation on the anode side of Design 1 (Fig. 6b). Due to the addition of heat reser-

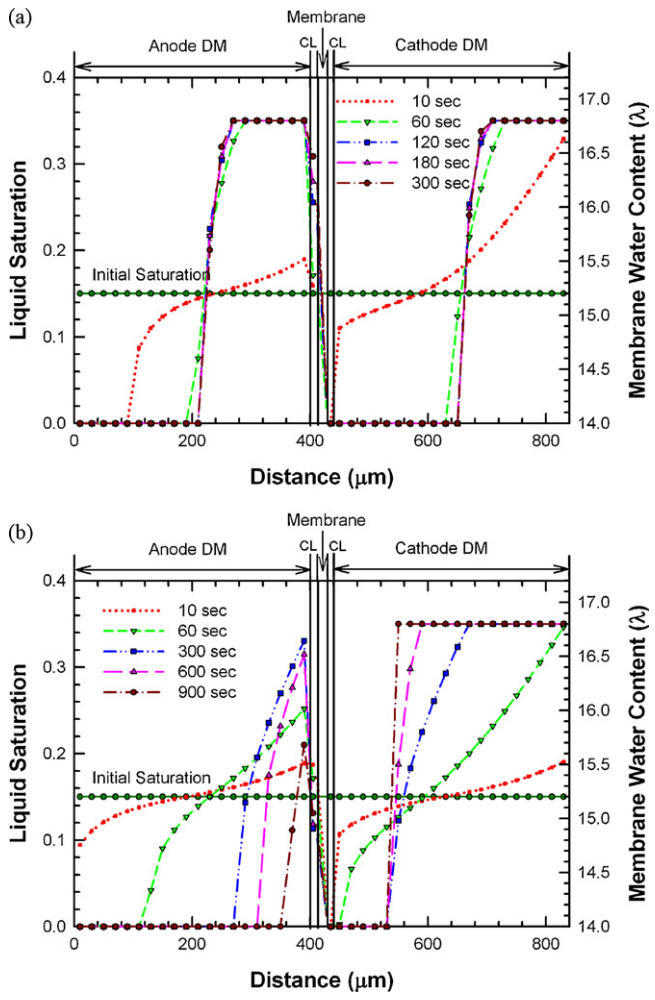

Fig. 5. Transient liquid saturation and water content distribution in the one-dimensional fuel cell simulation with negative thermo-osmotic diffusion coefficient, T_{avg} = 75 °C, land boundary condition (a) ΔT = 10 °C and (b) ΔT = 2 °C.

voir, the temperature gradient in the stack is increased in Design 2. Stack dimensions for both designs are listed in Table 1. Table 2 lists the stack material properties used in the stack thermal model. Both stack designs were cooled from 65 °C to room temperature by natural cooling (from anode end plate).

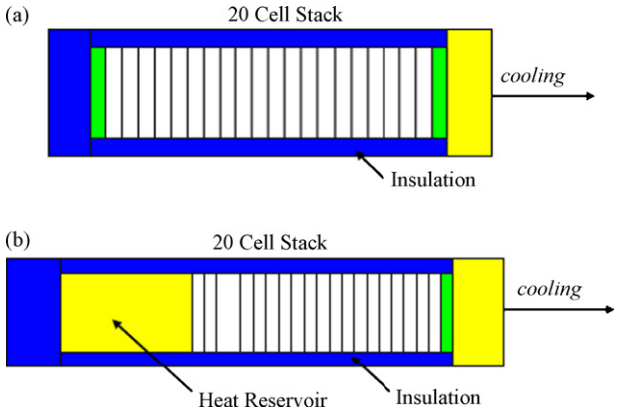

Fig. 6. Schematic of stack design to use temperature gradient to drain water [11] (a) Design 1: fuel cell stack insulated on all side except one stack end and (b) Design 2: new fuel cell stack design with heat reservoir between anode insulation and end plate.

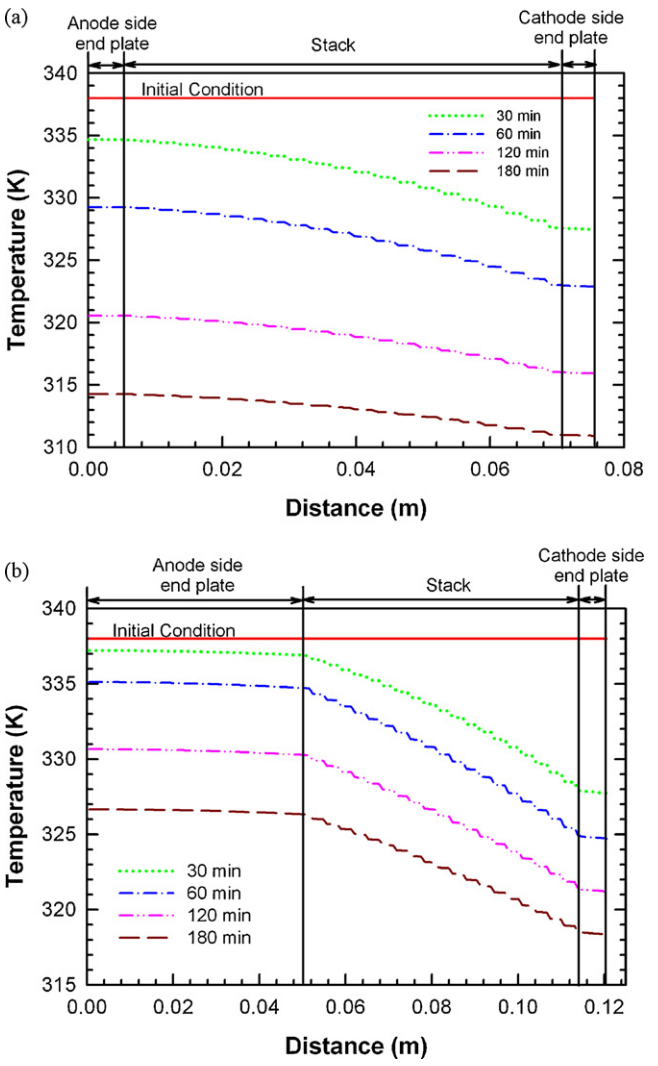

Fig. 7. Transient temperature distribution in a 20-cell PEFC stack during shutdown (natural cooling): (a) conventional stack insulated from all side except cathode end plate (Design 1) and (b) stack design with high thermal mass on anode end plate [11] (Design 2).

Fig. 7(a) and (b) shows the transient stack temperature profile for both stack designs. Stack simulations were performed to simulate 12 h after shutdown, but temperature profiles are shown only for the first 3 h for brevity. It can be easily seen from the plot that the net temperature gradient across cells in stack Design 2 is almost two times higher as compared to the Design 1. After 30 min of shutdown, the average temperature difference across the cells in the stack was ~6 °C for Design 1 and ~10 °C for Design 2. The two key parameters for temperature driven phase-change water transport are average temperature and temperature gradient [13]. It is quite evident from Fig. 6 that cells in Design 2 have higher average temperature as compared to Design 1. To investigate the temperature gradient, the variation of temperature difference across anode/cathode end cell with time for both stack designs is shown in Fig. 8. For the anode end cell (cell 1), the maximum temperature difference (ΔT) for Design 2 (~0.3 °C) is almost three times more than Design 1 (~0.1 °C). On the other hand, for the cathode end cell (cell 20), the maximum ΔT is almost the same (~0.55 °C) for both stack designs. However, after achieving the maximum ΔT, the rate of decrease of ΔT for cathode end cell in Design 2 is substantially lower than Design 1. Thus, Design 2 not only amplifies the temperature gradient for anode end cell, but it also increases the cell

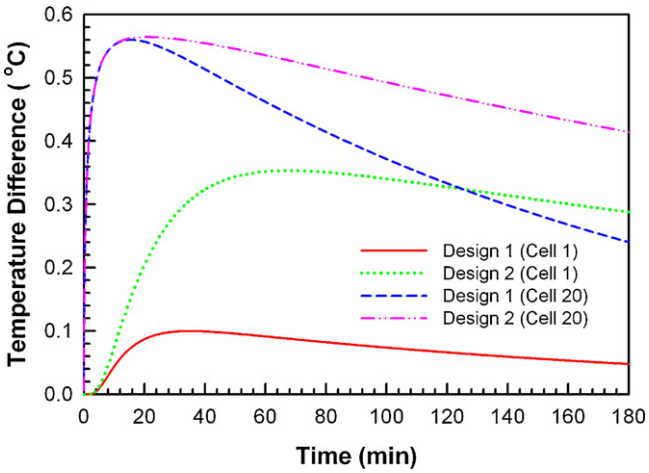

Fig. 8. Transient temperature difference across anode end cell (cell 1) and cathode end cell (cell 20) for both stack designs.

average temperature for both anode/cathode end cells. Both effects enhance water motion via phase-change induced flow effects.

3.4. End cell water distribution

To investigate the detailed water transport in the end cell during shutdown, the temperature boundary condition was derived from the stack model results. Single cell simulations were performed with constant initial temperature of 65 °C, liquid saturation of 0.15 in DM and CL, and membrane water content ($\lambda = H_2O/SO_3^-$) of 15.2. For detailed comparison, end cell results are presented for both land and channel boundary condition with identical temperature boundary condition. It should be noted that in the real scenario land and channel may have different temperature boundaries which may complicate the water transport somewhat.

Fig. 9 shows the rate of decrease of average saturation in anode/cathode end cell for both stack designs. Note that this is the maximum value, since we are assuming zero capillary pressure in the channel. The assumption of zero capillary pressure will not be true if there is a droplet in the channel because of drainage from diffusion media. For the cathode end cell, water drainage rate is almost the same for both stack designs for first 45 min after shutdown. Afterwards, water drainage rate decreases slightly for Design 1 end cell due to lower temperature gradient as compared to Design 2 end cell (Fig. 8). On the other hand, the Design 2 anode end cell

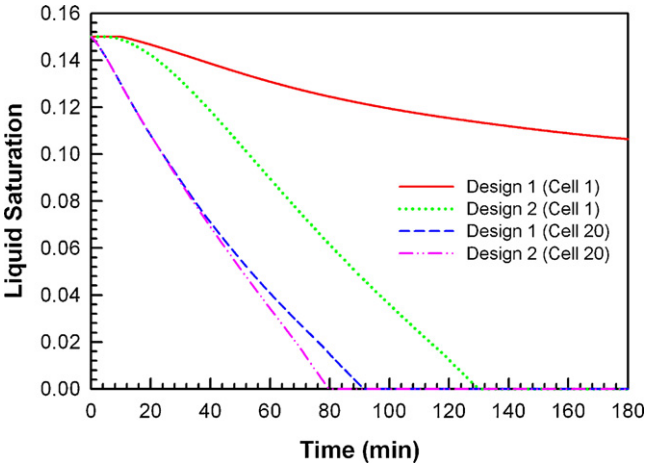

Fig. 9. Rate of water removal in porous diffusion media in anode end cell (cell 1) and cathode end cell (cell 20) for both stack designs.

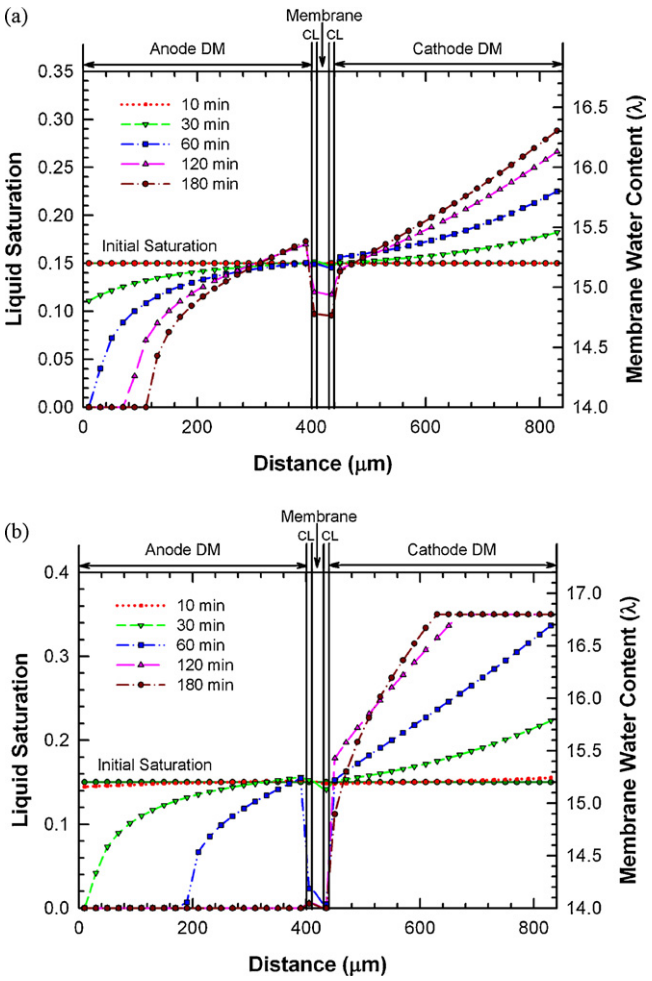

Fig. 10. Transient liquid saturation distribution in the anode end cell for both stack designs with land boundary condition (a) Design 1 and (b) Design 2.

perform substantially better than Design 1. Water drainage rate increases almost three to four times from Design 1. The improvement in the drainage rate for Design 2 anode end cell is a combined effect of high average temperature and gradient. This observation is consistent with experimental observation by Bradean et al. [11], and also qualitatively validates the integrated modeling approach. It should be noted that exact quantitative match is very difficult to obtain due to the unavailability of stack design and dimensions as well as limitations of the two-phase model. In this shutdown experiment, negative membrane thermo-osmotic diffusion was considered. This implies that there will be always some residual amount of water at anode catalyst layer, resulting from the balance of thermo-osmosis and diffusion flux in membrane. As temperature decreases, thermo-osmotic flux also decreases. Thus, the residual water at anode the catalyst layer decreases. After 3 h of shutdown, liquid saturation was reduced to less than 0.01 for all cases except the Design 1 anode end cell, as shown in Figs. 10 and 11.

Figs. 10 and 11 show the detailed liquid saturation distribution in the anode end cell with land and channel boundary condition, respectively. For the land boundary condition, water evaporates at higher temperature and diffuses towards the right side (lower temperature) and condenses underneath the land. Eventually, a balance of backward capillary flux and forward diffusion flux is achieved. On the other hand, for the channel boundary condition, water vapor escapes from the right side, thus drains liquid water from the fuel cell. The water drainage rate presented in Fig. 9 was derived from the simulations with channel boundary

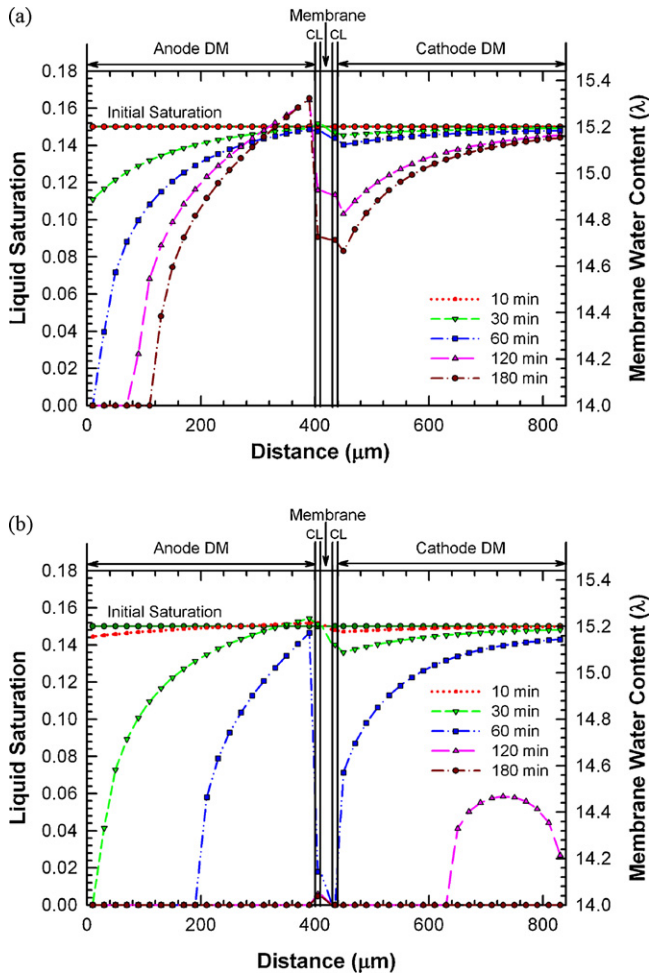

Fig. 11. Transient liquid saturation distribution in the anode end cell for both stack designs with channel boundary condition (a) Design 1 and (b) Design 2.

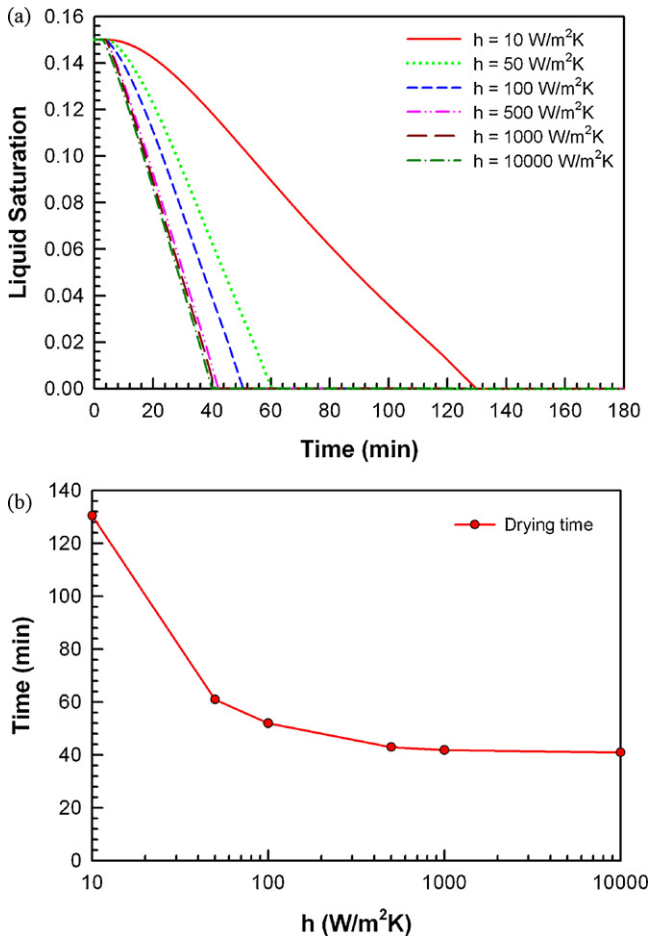

Fig. 12. (a) Rate of water removal in porous media in anode end cell (cell 1) for Design 2 with different cooling rate on right end plate and (b) variation of porous media drying time with cooling rate.

(Fig. 11). This analysis indicates that a change in the stack design can enhance the stack temperature gradient and increase the water removal rate.

3.5. *Effect of cooling rate*

All the above simulations were presented with natural cooling on the right end plate (cathode side) for the stack. Fig. 12 shows the improvement in the dry-out time for the Design 2 anode end cell with an increase in the cooling rate (convective heat transfer coefficient on right end plate: h). Here, the dry-out time is defined as the time for average saturation in the fuel cell diffusion media to become less than 0.01. This condition is chosen because, due to the negative membrane thermo-osmotic diffusion coefficient, it is not possible to fully drain the liquid water using the temperature gradient method. Fig. 12(a) shows the drainage rate for varying cooling rate, h, varying from 10 to 10,000 $W\,m^{-2}\,K^{-1}$. Drainage rate increases with increase in h from 10 to 50 $W\,m^{-2}\,K^{-1}$. At $h = 10\,W\,m^{-2}\,K^{-1}$, the average liquid saturation was reduced to its minimum value in 130 min. However, for $h = 50\,W\,m^{-2}\,K^{-1}$, it took only 60 min to drain the same amount of liquid water. It should be noted that the drainage of the water from the porous media is into the channels, which would ultimately need to be drained as well before freeze. This can be accomplished with a rapid purge of circulating gas, or with gravity forces, depending on the particular design. Afterwards, the rate of increase in water removal is significantly decreased and reaches almost an asymptotic value for h greater than $100\,W\,m^{-2}\,K^{-1}$, and is shown in Fig. 12(b). The increase in cooling rate (h) is proportional to the parasitic losses in the fuel cell system, implying this approach may decrease the overall fuel cell system efficiency. The purpose of use of thermal driven phase-change flux is to drain the liquid water from the fuel cell with minimum parasitic loss. Additionally, forced cooling may also result in reaching the ambient temperature at a faster rate as compared to the natural cooled stack design or conventional stack design. So, in sub-zero environment, a forced cooling stack design may end up in having more cold start cycle than conventional stack and can impact fuel cell durability. Thus, with a forced cooling stack design, a careful analysis must be done in enhancement of drainage (saving in parasitic losses), and additional energy required and its impact on fuel cell durability.

Depending on the location of a particular fuel cell in a stack, the anode or cathode side may be the colder location during shutdown, and a scenario with a temperature gradient can exist. A key to minimize the residual water at the cathode catalyst layer is to maintain the relative balance of phase-change induced flux in DM, and net balance of thermo-osmotic flux and diffusion flux in the membrane. The goal is to fully drain the electrode at shutdown before a frozen condition is reached. The reader should also note that these results are investigated for the current specific stack design and may not be directly applicable to others stack design. Stack design for automobile and other application may need to be changed to use temperature driven flow to reduce the residual water. But this work clearly demonstrates that by changing

the stack design a modest temperature gradient can be achieved to increase the water drainage at the electrode before cold conditions (a high enough gradient to move water, but not enough for thermo-osmotic flux to overcome diffusive drainage), thus proper shutdown can be achieved. Thus, by reducing residual water, both cold start performance and freeze-damage can be improved.

4. Conclusions

In this work, an integrated modeling approach is presented to investigate the concept of using controlled temperature gradients to non-parasitically remove excess water during PEFC shutdown. Two mathematical models: a two-phase single cell model and a stack level thermal model have been developed and integrated thru boundary conditions. The stack level model is a transient thermal model which provides detailed stack temperature distribution. The single cell level model is a two-phase unit cell model and is capable to predict the detailed saturation and thermal profile in the PEFC components. The key features of the two-phase single cell model are incorporation of phase-change induced flow in the porous media, and thermo-osmotic flux in the polymer membrane. To integrate both models, the single cell model is used to estimate the local water distribution with land/channel boundary condition, and the stack thermal model provided the transient temperature boundary condition to simulate any cell in the stack.

Model results indicate that a favorable temperature gradient can be formed in the stack to enhance the water drainage rate with a high impact in the anode end cells by changing the stack design to promote an internal temperature gradient during shutdown. It was shown that water drainage rate can be increased by three to four times by adding a heat reservoir at the anode end plate. This favorable temperature gradient (or drainage rate) can be further enhanced by forced cooling on the cathode side of the stack. It was found that water drainage rate reaches an asymptotic value for a cooling rate higher than h $100\,W\,m^{-2}\,K^{-1}$. However, a forced cooling stack design may have adverse impact on overall system efficiency and fuel cell durability as compared to conventional stack design. Ultimately, the results of this work can be used to improve stack design and develop less parasitic shutdown protocol to minimize the residual water in the fuel cell materials after shutdown.

Acknowledgement

This work was partially supported by the Advanced Technology Center, R&D Division for Hyundai Motor Company (HMC) & Kia Motors Corporation (KMC). Additional funding was provided by NSF CAREER Award no: 0644811. The authors thank Dr. Soowhan Kim for providing the NR images and useful discussion about thermo-osmosis, and Dr. D. S. Hussey and Dr. D. L. Jacobson for assistance in using the NR facility at NIST.

References

[1] R. Mukundan, Y.S. Kim, F. Garzon, B. Pivovar, ECS Trans. 1 (8) (2006) 403–413.
[2] F. Garzon, Y.S. Kim, M. Rangachary, B. Pivovar, DOE Hydrogen Program Review, Crystal City, VA, May 16–19, 2006, http://www1.eere.energy.gov/hydrogenandfuelcells/.
[3] Y. Wang, J. Electrochem. Soc. 154 (10) (2007) B1041–B1048.
[4] S. Kim, M.M. Mench, J. Power Sources 174 (2007) 206–220.
[5] S. He, S.H. Kim, M.M. Mench, J. Electrochem. Soc. 154 (10) (2007) B1024–B1033.
[6] S. He, J.H. Lee, M.M. Mench, J. Electrochem. Soc. 154 (12) (2007) B1227–B1236.
[7] S. He, M.M. Mench, J. Electrochem. Soc. 153 (9) (2006) A1724–A1731.
[8] M. Khandelwal, S. Lee, M.M. Mench, J. Power Sources 172 (2007) 816–830.
[9] M. Khandelwal, J.J. Ko, M.M. Mench, ECS Trans. 11 (1) (2007) 553–563.
[10] M. Khandelwal, J.H. Lee, M.M. Mench, Proceedings of the 5th ASME International Conference on Fuel Cell Science Engineering and Technology, New York, USA, June 18–20, 2007.
[11] R. Bradean, H. Haas, K. Eggen, C. Richards, T. Vrba, ECS Trans. 3 (1) (2006) 1159–1168.
[12] M.L. Perry, T. Patterson, J. O'Neil, Proceedings of the 5th ASME International Conference on Fuel Cell Science Engineering and Technology, New York, June 18-20, 2007.
[13] M. Khandelwal, S.H. Lee, M.M. Mench, J. Electrochem. Soc. 156 (6) (2009) B703–B715.
[14] M. Khandelwal, S.H. Lee, Y.J. Son, M.M. Mench, ECS Trans. 13 (28) (2008) 75–87.
[15] A.Z. Weber, J. Newman, J. Electrochem. Soc. 153 (12) (2006) A2205–A2214.
[16] A.Z. Weber, Proceedings of the 214th ECS meeting, Honolulu, HI, October 12–17, 2008.
[17] T.E. Springer, T.A. Zawodzinski, S. Gottesfeld, J. Electrochem. Soc. 138 (8) (1991) 2334–2342.
[18] G.J.M. Janssen, J. Electrochem. Soc. 148 (12) (2001) A1313–A1323.
[19] A.A. Kulikovsky, J. Electrochem. Soc. 150 (11) (2003) A1432–A1439.
[20] M. Tasaka, T. Suzuki, R. Kiyono, M. Hamada, K. Yoshie, J. Phys. Chem. 100 (1996) 16361–16364.
[21] J.P.G. Villaluenga, B. Seoane, V.M. Barragan, C. Ruiz-Bauza, J. Membr. Sci. 274 (2006) 116–122.
[22] D.M. Bernardi, W. Verbrugge, J. Electrochem. Soc. 139 (9) (1992) 2477–2491.
[23] A.Z. Weber, R.M. Darling, J. Newman, J. Electrochem. Soc. 151 (10) (2004) A1715–A1727.
[24] S.C. Yeo, A. Eisenberg, J. Appl. Polym. Sci. 21 (4) (1977) 875–898.
[25] S. Kim, M.M. Mench, J. Membr. Sci. 328 (2009) 113–120.
[26] F.P. Incropera, D.P. DeWitt, Fundamentals of Heat and Mass Transfer, 4th ed., John Wiley & Sons, 1996.
[27] M. Khandelwal, M.M. Mench, J. Power Sources 161 (2006) 1106–1115.
[28] M. Khandelwal, PhD Dissertation, The Pennsylvania State University (2009).
[29] A. Turhan, S. Kim, M. Hatzell, M.M. Mench, Electrochimica Acta 55 (8) (2010) 2734–2745.